Image Formation in Vibro-acoustography with Sector Array Transducers

Glauber T. Silva, Alejandro C. Frery,
and Eliana Almeida
Universidade Federal de Alagoas
Dep. de Tecnologia da Informação
57072-970 Maceió, AL – Brazil
glauber@tci.ufal.br

Shigao Chen, Mostafa Fatemi,
and James F. Greenleaf
Mayo Clinic College of Medicine
Department of Physiology and Biophysics
55905 Rochester, MN – USA

Abstract

This paper presents the image formation process in vibro-acoustography for systems based on sector array transducers. These transducers are an alternative to annular concave transducers. They represent an innovative technique deserving detailed assessment in vibro-acoustography applications. The system point-spread function (PSF) is defined in terms of the acoustic emission of a point-target in response to the dynamic ultrasound radiation force. This force is produced by two overlapping ultrasound beams. We calculate the radiation force on the target in a nonviscous fluid using the plane wave approximation for the ultrasound beams. The beamforming of sector array transducers is analyzed through linear acoustics. An expression for the velocity potential produced by sector arrays is derived, and the vibro-acoustography PSF is evaluated numerically. An experimental setup is design to validate the theory; the comparison is made using location and amplitude of sidelobes and spatial resolution defined by the PSF. Results show that the computed PSF is in full agreement with the PSF obtained experimentally.

1. Introduction

Vibro-acoustography is a relatively new imaging technique that maps the vibro-acoustical response of an object to the dynamic ultrasound radiation force [1]. This force is a phenomenon produced by the transference of the wave momentum to an object or propagating medium. Reviews of this phenomenon can be found in [2, 3, 4].

Dynamic radiation force can be produced by two co-focused continuous-wave (CW) ultrasound beams (dual beam mode) at slightly different frequencies. Typical frequencies used in vibro-acoustography are around 1–10 MHz with the difference frequency between 1–100 kHz. An object placed in the joint focal zone is subjected to the dynamic radiation force at the difference frequency. In response to the radiation force, the object vibrates emitting an acoustic field (acoustic emission). A detector can measure the acoustic emission produced by the object. As the focal point of the ultrasound beams is scanned across the object, the amplitude (or phase, in some cases) of the measured signal is used to produce an image of the object. Vibro-acoustography has been studied as a potential imaging technique in a myriad of clinical applications and nondestructive material evaluation [5].

Beamforming in vibro-acoustography shares similarities with conventional ultrasound (B-mode) imaging. However, some conceptual differences should be pointed out, namely:

- Vibro-acoustography images are generated by two intersecting CW-ultrasound beams, while B-mode uses only one pulsed ultrasound beam.
- The depth resolution in B-mode depends on the transmitted pulse duration, while in vibro-acoustography- it is related to the depth of the overlapping region of the two ultrasound beams.
- Vibro-acoustography uses narrow-band signals, while ultrasound systems are based on broad-band transmitted pulses.
- In most applications, ultrasound systems acquire data along one line in depth at a time (the so-called 'A-line'), while vibro-acoustography incrementally scans a region by collecting data of each point of the region at a time.

Furthermore, vibro-acoustography produces speckless images. In spite of all differences, the common goal of B-mode ultrasound and vibro-acoustography is to achieve narrow beams with low sidelobes and minor effects of grating lobes in order to produce high-quality images.

Proceedings of the XVII Brazilian Symposium on Computer Graphics and Image Processing (SIBGRAPI'04)
1530-1834/04 $ 20.00 IEEE

Beamforming and image formation in vibro-acoustography have been studied for systems based on two-element annular concave [6, 7] and linear array [8] transducers. Concave transducers have the unique advantage of producing highly focused and symmetric ultrasound beams; however, these transducers have fixed focus with concentric sidelobes below -19 dB. Linear array transducers can steer and focus the produced ultrasound beam by electronically de-phasing each array element.

Despite drawbacks, concave transducers have much simpler electronic circuitry compared to linear arrays. Therefore, these transducers might be suitable for simple vibro-acoustography systems applied for non-destructive material evaluation or *in vitro* biological tissue experiments. Sector array transducer is an alternative to two-element annular concave array transducer with same characteristics. In fact, a sector array is a concave transducer whose aperture is divided in sectors that can be electronically driven independently. Sector array transducer in vibro-acoustography was used to study tissue stiffness variation with temperature [9].

So far, vibro-acoustography systems based on sector array transducers have not been studied at all. In this work, we present a theory of vibro-acoustography image formation. The system point-spread function (PSF) is obtained as the product of the velocity potential of the two ultrasound sources. The theory is applied by the first time to a system based on a sector array transducer. An expression of the velocity potential produced by a sector array is derived, and the vibro-acoustography PSF is evaluated numerically. The theory is validated by an experiment using a small steel sphere as a point-target to measure the PSF. We present experimental results that are in full agreement with the theory.

2. System description

Figure 1 shows a vibro-acoustography system. A two-element transducer is used to produce the dynamic radiation force on the object. The scanning motion is done by moving the vibro-acoustography transducer with step motors. Two function generators produce the sinusoidal driving signals at frequencies ω_a and ω_b. The mixer generates a harmonic signal at the difference frequency $\Delta\omega$, which is used as a the reference signal in the lock-in amplifier. The signal detected by the hydrophone is filtered at $\Delta\omega$ by the lock-in. An A/D conversor digitalizes the analog signal. The digital signal is stored and used to form the image.

Figure 2(a) shows a breast phantom with lesion-like inclusions. Figure 2(b) shows the vibro-acoustography image of the selected area in Figure 2(a), where the inclusions are evident. The system employed a two-element annular concave transducer with resolution 1.6×1.6 mm.

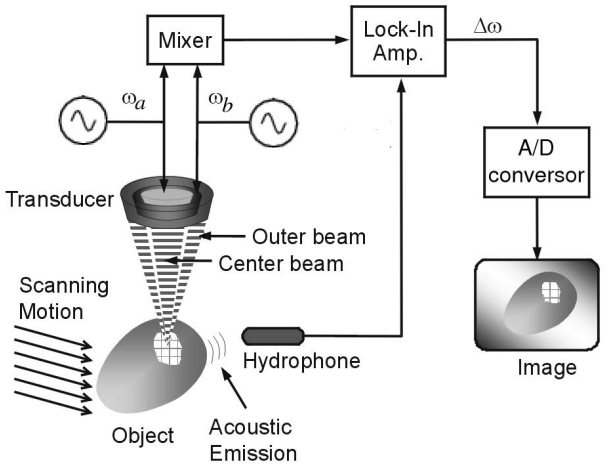

Figure 1. The vibro-acoustography imaging system.

3. Theory

3.1. Ultrasound radiation force

Assume that the propagating medium is an infinite, homogeneous, and lossless fluid with density ρ_0 and speed of sound c_0. In a lossless medium, ultrasound waves can be fully described in terms of the velocity potential $\phi(\mathbf{r}, t)$, where $\mathbf{r} = (x, y, z) \in \mathbb{R}^3$ is the position vector and $t \in \mathbb{R}$ is the time. The particle velocity in the medium is given by $\mathbf{v} = -\nabla\phi$, where ∇ is the gradient operator. In terms of the velocity potential, the acoustic pressure is $p = \rho_0(\partial\phi/\partial t)$.

It is known that an ultrasound plane wave exerts a radiation force upon a target placed in the wave path. Westervelt [10] showed that the normal component of the radiation force caused by a collimated plane wave striking an object is given by

$$f = d_c\langle E\rangle, \tag{1}$$

where d_c is a function of the cross-sections of the scattering and absorption by the object per unit area, and $\langle E\rangle$ is the energy density of the incident sound beam averaged over an infinite time interval.

In vibro-acoustography, two intersecting ultrasound beams focused at the same point in space produce a dynamic radiation force on an object. Each source is driven by a CW-signal with angular frequencies $\omega_a = \omega_0 + \Delta\omega/2$ and $\omega_b = \omega_0 - \Delta\omega/2$, respectively. The quantities ω_0 and $\Delta\omega$ are the center and difference frequencies, with $\Delta\omega \ll \omega_0$. In response, the object vibrates emitting an acoustic field.

Using the superposition principle, the velocity potential of the incident ultrasound beam can be written as

$$\phi(\mathbf{r}, t) = \hat{\phi}_a(\mathbf{r})e^{j\omega_a t} + \hat{\phi}_b(\mathbf{r})e^{j\omega_b t}, \tag{2}$$

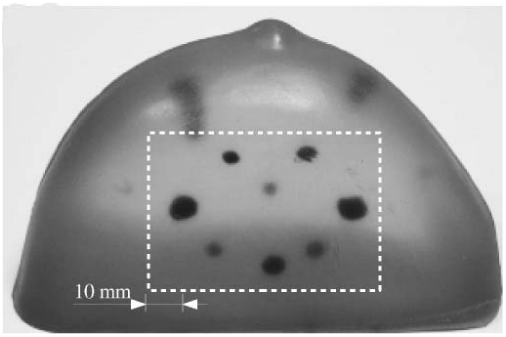

(a) Breast phantom with inclusions.

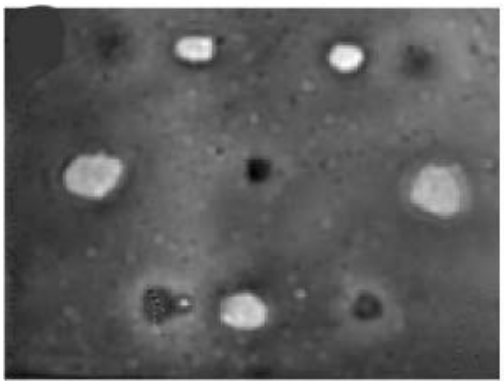

(b) Vibro-acoustography of the phantom.

Figure 2. Breast phantom with inclusions and its vibro-acoustography image.

where j is the imaginary unit, and $\hat{\phi}_a$ and $\hat{\phi}_b$ are the complex amplitude of the ultrasound beams. We assume that the resulting ultrasound beam described in Eq. (2) behaves as a plane wave in the vicinity of the system focal zone. Thus, the instantaneous ultrasound energy density in the focal zone is given by

$$E(t) = \frac{p^2}{\rho_0 c_0^2} = \frac{\rho_0}{c_0^2} \Re \left\{ \left(\frac{\partial \phi}{\partial t} \right)^2 \right\}, \qquad (3)$$

where $\Re\{\cdot\}$ denotes the real-part of a complex quantity. From Eq. (2) one can show that the instantaneous ultrasound energy has a harmonic component at the difference frequency $\Delta\omega$. To obtain the dynamic radiation force at $\Delta\omega$ from Eq. (1), we define the short-term time-average of a function $s(t)$ as follows:

$$\langle s \rangle_T \equiv \frac{1}{T} \int_{t-T/2}^{t+T/2} s(t')dt', \qquad (4)$$

where T is an arbitrary time interval. Note that if $T \to \infty$ we recover the usual time-average definition.

The short-term time average of E is obtained by substituting (2) into (3) with T satisfying $\frac{2\pi}{\omega_0} \ll T \ll \frac{4\pi}{\Delta\omega}$. Hence, the dynamic energy density at the difference frequency $\Delta\omega$ is given by

$$E_d(\mathbf{r}, t) = \frac{\rho_0 \omega_a \omega_b}{c_0^2} \Re \left\{ \hat{\phi}_a(\mathbf{r}) \hat{\phi}_b^*(\mathbf{r}) e^{j\Delta\omega t} \right\}. \qquad (5)$$

A vibro-acoustography imaging system can be characterized by its PSF, which is defined as the response of the system to a point-target. In vibro-acoustography, the PSF depends on the acoustic emission of the point-target, which is caused by the dynamic radiation force. In general, the radiation force exerted on a target by an ultrasound beam is a three-dimensional vector quantity. However, if the incident beam is sufficiently collimated, i.e., the variation on direction transverse to the wave propagation direction is negligible, then we can use Eq. (1). In this approach, we exchange the usual time-average definition by the short-term time-average. Therefore, replacing Eq. (5) into Eq. (1), we obtain (in complex notation) the dynamic radiation force on the point-target localized at $\mathbf{r}_1$ as

$$\begin{aligned} f_d(\mathbf{r}_1, t) &= \hat{f}_{\Delta\omega} e^{j\Delta\omega t} \\ &= \frac{\rho_0 \omega_a \omega_b}{c_0^2} d_c(\mathbf{r}_1) \hat{\phi}_a(\mathbf{r}_1) \hat{\phi}_b^*(\mathbf{r}_1) e^{j\Delta\omega t}, \end{aligned} \qquad (6)$$

where $\hat{f}_{\Delta\omega}$ is the complex amplitude of the force.

3.2. Acoustic emission

Let us analyze the response of an object to the dynamic radiation force. An object submitted to a dynamic force responds to the force according to its mechanical properties and boundary conditions. A simple example is tapping a drum with a time-varying force. The mechanical properties of the drum's membrane such as elasticity, tension and density, plus boundary conditions produce a specific sound pitch. The boundary conditions of the drum are related to its geometric shape. Furthermore, the position where the force is applied also influences the sound produced by the membrane. The example of the drum can be adapted to understand the response of objects to the dynamic radiation force.

In vibro-acoustography, the dynamic radiation force "taps" an object embedded in the propagating medium. In response, the object emits an acoustic field (acoustic emission), which depends on the object's mechanical properties and boundary conditions. The acoustic emission is detected and used to synthesize an image of the

object. We are, thus, interested in calculating the acoustic emission of a point-target.

The point-target is modeled as a vibrating sphere of radius a, with $\Delta ka \ll 1$ ($\Delta k = \Delta\omega/c_0$). The sphere vibrates around the origin of the coordinate system with a velocity $\hat{v}_{\Delta\omega}e^{j\Delta\omega t}$ in the z-direction. The vibrating sphere should have some sort of restoration mechanism, such as a mass-spring system, to keep it oscillating around its equilibrium position. One can show that the amplitude of the acoustic field generated by the sphere in the far-field is given, in spherical coordinates, by

$$\hat{p}_{\Delta\omega} = 4\pi\rho_0 c_0 \hat{v}_{\Delta\omega}\frac{a\cos\theta}{1-j\Delta ka}\frac{e^{-j\Delta kr}}{4\pi r}. \tag{7}$$

The velocity amplitude of the vibrating sphere caused by the dynamic radiation force can be described through the mechanical impedance $\hat{z}_{\Delta\omega}$ as

$$\hat{v}_{\Delta\omega} = \frac{\hat{f}_{\Delta\omega}}{\hat{z}_{\Delta\omega}}. \tag{8}$$

Defining the acoustic outflow (the volume of the medium which is displaced per unit time due to the object vibration) per unit force of the sphere as $\hat{q}_{\Delta\omega} = 2\pi a^2/\hat{z}_{\Delta\omega}$, we can rewrite Eq. (7) as

$$\hat{p}_{\Delta\omega} = 2\rho_0 c_0 \hat{f}_{\Delta\omega}\hat{q}_{\Delta\omega}\frac{\cos\theta}{a(1-j\Delta ka)}\frac{e^{-j\Delta kr}}{4\pi r}. \tag{9}$$

The acoustic emission in Eq. (9) can be generalized for a point-target located at an arbitrary position $\mathbf{r}_1$. If we detect the emission on a position $\mathbf{r}_2$, Eq. (9) becomes

$$\hat{p}_{\Delta\omega}(\mathbf{r}_2 \mid \mathbf{r}_1) = 4\rho_0 c_0^2 \hat{f}_{\Delta\omega}(\mathbf{r}_1)\hat{q}_{\Delta\omega}(\mathbf{r}_1)\hat{g}_{\Delta\omega}(\mathbf{r}_2 \mid \mathbf{r}_1), \tag{10}$$

where

$$\hat{g}_{\Delta\omega}(\mathbf{r}_2 \mid \mathbf{r}_1) = \frac{\cos\theta_{12} G_{\Delta\omega}(\mathbf{r}_2 \mid \mathbf{r}_1)}{2c_0 a(1-j\Delta ka)}, \tag{11}$$

and θ_{12} is the angle between the vectors $\mathbf{r}_1$ and $\mathbf{r}_2$. The quantity $G_{\Delta\omega}$ is the Green's function of the acoustic wave equation for an infinite medium, which is given by

$$G_{\Delta\omega}(\mathbf{r}_2 \mid \mathbf{r}_1) = \frac{\exp(-j\Delta k|\mathbf{r}_2 - \mathbf{r}_1|)}{4\pi|\mathbf{r}_2 - \mathbf{r}_1|}. \tag{12}$$

The function $\hat{g}_{\Delta\omega}$ is independent of the mechanical properties of target; it depends only on the medium characteristics and boundary conditions. The function $\hat{q}_{\Delta\omega}$ describes the object characteristics at the frequency $\Delta\omega$. Equation (10) was obtained in [6] considering a piston in a semi-infinite space as a point-target.

Substituting $\hat{f}_{\Delta\omega}$ from Eq. (6) into Eq. (10) yields

$$\begin{aligned}\hat{p}_{\Delta\omega}(\mathbf{r}_2|\mathbf{r}_1) = {} & 4\rho_0^2\omega_a\omega_b d_c(\mathbf{r}_1)\hat{q}_{\Delta\omega}(\mathbf{r}_1)\cdot \\ & \cdot\hat{\phi}_a(\mathbf{r}_1)\hat{\phi}_b^*(\mathbf{r}_1)\hat{g}_{\Delta\omega}(\mathbf{r}_2 \mid \mathbf{r}_1)\end{aligned} \tag{13}$$

Eq. (13) gives the acoustic emission in terms of the incident ultrasound amplitude functions $\hat{\phi}_a$ and $\hat{\phi}_b$. This is useful for vibro-acoustography beamforming as we shall see later in this article.

3.3. Image formation

Imaging techniques based on ultrasound waves, such as ultrasonography and vibro-acoustography, illuminate the region of interest (ROI) by means of focused ultrasound beams. To form an image, the ultrasound beam should scan the ROI, and the scanning process can be accomplished either by mechanically moving the transducer or electronically steering the beam by using array transducers. Image synthesis in vibro-acoustography depends upon the acoustic emission of the ROI.

To define the image of an object we need to represent the object through a function. Referring to Eq. (13), the terms that depend on the object characteristics are d_c and $\hat{q}_{\Delta\omega}$. Hence, the object function is defined in terms of these quantities spatially distributed as

$$\xi(\mathbf{r}) \equiv d_c(\mathbf{r})\hat{q}_{\Delta\omega}(\mathbf{r}). \tag{14}$$

It is assumed that the acoustic emission of an extended body is a linear combination of the emission of every infinitesimal volume of the ROI. For an infinitesimal volume, the acoustic emission is given by Eq. (13). This allows us to define a point-target in terms of the three-dimensional impulse function as

$$\xi(\mathbf{r}) = \delta^{(3)}(\mathbf{r} - \mathbf{r}_1),$$

where $\delta^{(3)}$ is the 3D-Dirac delta function. To calculate the system PSF, we consider that the two ultrasound beams are focused at a fixed point $\mathbf{r}_0$. The point-target can vary its position in the vicinity of $\mathbf{r}_0$, and this neighborhood is assumed to be small enough such that $\hat{g}_{\Delta\omega}$ remains unchanged. Thus, the normalized PSF of a vibro-acoustography imaging system is defined in terms of the amplitude of Eq. (13) as

$$h(\mathbf{r} \mid \mathbf{r}_0) = A\hat{\phi}_a(\mathbf{r})\hat{\phi}_b^*(\mathbf{r}), \tag{15}$$

where $A = [\hat{\phi}_a(\mathbf{r}_0)\hat{\phi}_b^*(\mathbf{r}_0)]^{-1}$. Note that the subindex of $\mathbf{r}_1$ was dropped in Eq. (15). The PSF depends on the system focal point $\mathbf{r}_0$ because the functions $\hat{\phi}_a^*$ and $\hat{\phi}_b^*$ depend also on $\mathbf{r}_0$. The system is, thus, spatially shift-variant. The vibro-acoustography PSF is a complex function of the three-dimensional coordinates. Equation (15) is valid for transducers of any geometric shape.

The *spatial resolution* of the system is arbitrarily defined as the volume enclosed by the PSF magnitude at -6 dB.

3.4. Beamforming for sector array transducer

Beamforming in vibro-acoustography involves the formation of CW-ultrasound focused beams. The theory of ultrasound radiation from baffled pistons based on linear acoustics is used to model the vibro-acoustography beamforming [6].

An ultrasound transducer can be modeled as a piston mounted in an infinite extended planar rigid baffle. It is assumed that the baffle is immovable, hence only the piston can move in its normal direction. The pressure field radiated by a piston mainly depends on its geometric shape and the normal velocity distribution applied on the piston surface.

Consider a problem of determining the pressure field at a spatial point in the half-space $z > 0$ resulting from the radiation of a piston with surface Ω mounted in a baffled plane at $z = 0$. This can be formulated as a classical boundary-value problem to solve the linear wave equation for the acoustic potential $\phi(\mathbf{r}, t)$. The mathematical specification of the boundary-value problem yields the following system of equations

$$\begin{aligned} \nabla^2\phi(\mathbf{r},t) - \frac{1}{c_0^2}\frac{\partial^2\phi(\mathbf{r},t)}{\partial t^2} = 0, &\quad \mathbf{r} \in \left\{\mathbb{R}^3; z > 0\right\}, \\ \frac{\partial\phi}{\partial z} = -v_n(\mathbf{r},t), &\quad \mathbf{r} \in \Omega, t > 0, \\ \phi(\mathbf{r},0) = \left.\frac{\partial\phi(\mathbf{r},t)}{\partial t}\right|_{t=0} = 0, &\quad \mathbf{r} \in \left\{\mathbb{R}^3; z > 0\right\}, \end{aligned}$$

where v_n is the normal component of the velocity field on the piston.

Vibro-acoustography applications require transducers driven by CW-signals. Thus, consider the normal component of the velocity on the surface of the piston as

$$v_n(t) = v_0 e^{j\omega_0 t}, \tag{16}$$

where v_0 is the amplitude of the oscillation and ω_0 is an arbitrary angular frequency. The solution of the boundary-value problem for Eq. (16) is provided by [11]

$$\phi(\mathbf{r},t) = 2v_0 e^{j\omega_0 t}\int_\Omega G_{\omega_0}(\mathbf{r}' \mid \mathbf{r})dS(\mathbf{r}'). \tag{17}$$

This equation can be understood as the *Huygens' principle* in which every element dS on the surface Ω is considered a point-source emitting an spherical wave described by G_{ω_0}. Eq. (17) is only valid for the potential of flat transducers in a planar rigid baffle. If the transducer is curved, the integral neglects the fact that a wave radiated from any part of the surface is diffracted by other parts of the transducer. This secondary diffraction effect is unimportant if the surface Ω is slightly curved and its dimensions are much larger than the ultrasound wavelength.

In the following we will derive the velocity potential produced by a symmetric pair of elements in a sector array transducer using Eq. (17).

Consider a sector array transducer with N elements. The amplitude of the velocity potential, $\hat{\phi}_n$, radiated by a symmetric pair (see Figure 3) of elements in a sector transducer in the focal plane ($z = z_0$) can be described by Eq. (17).

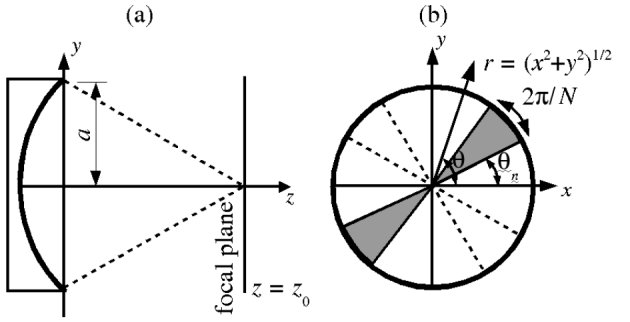

Figure 3. Sector array transducer: (a) lateral view; (b) a pair of elements.

We define the transducer f-number as $n_f = z_0/(2a)$, where a is the transducer aperture radius. In the *Fresnel approximation* ($a^2 \ll z_0^2$) one can show that the velocity potential amplitude at the focal plane due to the pair of elements in the sector array is given by Eq. (18).

It is useful to define the scaled wave-number as $\bar{k}_0 \equiv 2k_0/n_f$. One can show, from Eq. (18), that the velocity potential of the element pair is given by Eq. (21) in which J_n is the nth-order Bessel function of first-kind. The amplitude function $\hat{\phi}_0$ is

$$\hat{\phi}_0 = 2av_0 \exp\left[-jk_0\left(z_0 + \frac{r^2}{2z_0}\right)\right]. \tag{19}$$

The angular function s_{mn} is given by

$$s_{mn}(\theta) = \cos\left[m\left(\frac{\pi}{N} + \frac{2\pi n}{N} - \theta\right)\right]\sin\left(\frac{m\pi}{N}\right). \tag{20}$$

By setting $r = 0$ in Eq. (18), the velocity potential in the transducer axis (z-direction) can be written as

$$\begin{aligned} \hat{\phi}_n(z) = \frac{a^2 v_0}{\pi N z}\mathrm{sinc}\left[\frac{\bar{k}_0 a}{4\pi}\left(\frac{z_0}{z} - 1\right)\right] \\ \times \exp\left\{-jk_0\left[z + \frac{a^2}{4}\left(\frac{1}{z} - \frac{1}{z_0}\right)\right]\right\}, \end{aligned} \tag{22}$$

where $\mathrm{sinc}(x) = \sin(\pi x)/(\pi x)$.

Now consider a sector array transducer operating with N elements in dual beam mode. In this case, the elements

$$\hat{\phi}_n = \frac{\exp\left[-jk_0(z_0 + \frac{r^2}{2z_0})\right]}{\pi z_0} \int_0^a dr' r' \int_0^{2\pi/N} d\theta' \cos\left[k_0 r r' \cos(\theta' - \theta + 2\pi n/N)\right]. \quad (18)$$

$$\hat{\phi}_n(r,\theta) = \frac{\hat{\phi}_0}{\bar{k}_0 r}\left\{\frac{2\pi}{N}J_1(\bar{k}_0 r) + \sum_{\ell=0,m=1}^{\infty}\left[\frac{(-1)^m s_{(2m)n}(\theta)}{m}J_{2m+1}(\bar{k}_0 r) + \frac{4m}{\bar{k}_0 r}J_{2(m+\ell+1)}(\bar{k}_0 r)\right]\right\}, \quad n = 1, 2, 3, \ldots, N. \quad (21)$$

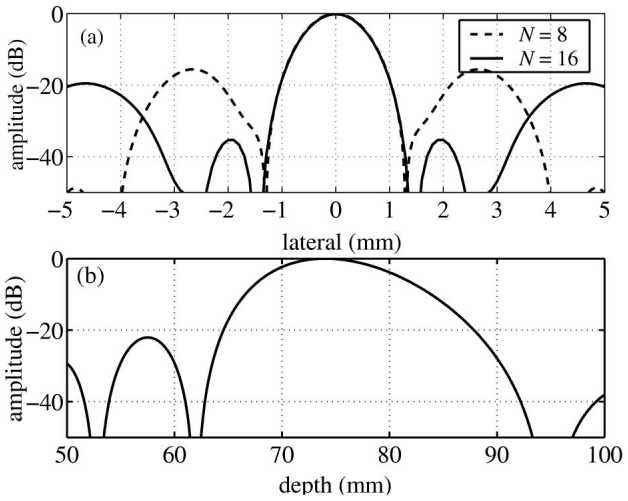

Figure 4. Plot of the PSF absolute value (a) laterally and (b) in depth.

are grouped in symmetric pairs. Each pair has angular frequency ω_a or ω_b, and they are alternated. Thus, when half of the pairs is at frequency ω_a the other half is at frequency ω_b. The amplitude of the velocity potential produced by the sector transducer can be expressed as

$$\hat{\phi} = \sum_{n=1}^{N/2}(\hat{\phi}_{2n-1}^{(a)} + \hat{\phi}_{2n}^{(b)}), \quad (23)$$

where the potentials $\hat{\phi}_n^{(a)}$ and $\hat{\phi}_n^{(b)}$ are given by Eq. (21) changing ω_0 for ω_a and ω_b, respectively. Hence, the vibro-acoustography PSF for the sector array is given, according to Eq. (15), by

$$h = A \sum_{m,n=1}^{N/2} \hat{\phi}_{2m-1}^{(a)} \hat{\phi}_{2n}^{(b)*}, \quad (24)$$

where A is the normalization constant.

4. Numerical evaluation and experiment

We evaluated the PSF of a sector array transducer with $N = 8$, radius $a = 23.5\,\text{mm}$, and focal distance $z_0 = 75\,\text{mm}$ in water ($c_0 = 1500\,\text{m/s}$). The element pairs in the transducer are driven alternately with frequencies $f_a = 2\,\text{MHz} + 5\,\text{kHz}$ and $f_b = 2\,\text{MHz} - 5\,\text{kHz}$. The PSF was numerically evaluated in MATLAB 6.5. Plots of the PSF absolute value in lateral direction and in depth are shown in Figure 4 for $N = 8, 16$. For $N = 8$ the sidelobes are below $-15.5\,\text{dB}$ and the transverse resolution is about $1.6 \times 1.6\,\text{mm}$. The depth-of-field of the system is $13.5\,\text{mm}$.

For $N = 16$ the first sidelobe in the PSF is under $-34\,\text{dB}$. However, the second sidelobe has level of about $-19\,\text{dB}$. Figure 5(a) shows the system PSF on the focal plane. The PSF has eight peripheral sidelobes circularly distributed around the mainlobe. Sidelobe peaks are separated by $\pi/4\,\text{rad}$.

An experimental setup was used to measure the sector array PSF on the system focal plane. A small steel sphere of about $600\,\mu\text{m}$ diameter attached to a latex sheet was used as a point-target in a water tank. A laser vibrometer measured the axial amplitude of the sphere vibration which is proportional to the system PSF. An 8-element sector array transducer of $23.5\,\text{mm}$ radius was used to image the sphere. The transducer operates in dual beam mode at $2\,\text{MHz}$ with difference frequency at $10\,\text{kHz}$. Figure 5(b) shows the surface plot of the measured PSF. Similarly to theoretical predictions, sidelobes are localized in eight spots separated by $\pi/4\,\text{rad}$ around the mainlobe. Sidelobe levels are below $-16\,\text{dB}$. Figure 6 shows the image of the measured PSF. The contour lines are the theoretical PSF at $-40\,\text{dB}$.

The criteria for the comparison of theoretical and experimental PSFs are spatial resolution, sidelobe position and level. As can be seen, the experimental result is in excellent agreement with the theory.

5. Discussion

We have presented image formation in vibro-acoustography for systems based on sector array transducers. The sys-

tem PSF was computed from the acoustic emission of a point-target in a lossless fluid using the plane wave approximation. Any influence of transverse forces is ignored in this approximation. In fact, transverse forces may appear on a target placed off the axis of the incident ultrasound beam. One effect caused by transverse forces is to change the direction of the object vibration. In the plane wave approximation, the force is always parallel to the direction of the ultrasound wave propagation. Modeling the radiation force due to an arbitrary ultrasound beam hitting a target in the three-dimensional space is out of the scope of this work.

The radiation force may be different depending on the medium attenuation. A propagating wave might be attenuated by absorption or scattering caused by medium inhomogeneities. Attenuation alters the results in at least two ways. The ultrasound wave traveling through an attenuating fluid exerts a radiation force on the medium [12] which gives rise to acoustic streaming. A lossy medium also attenuates the incident beam reducing the radiation force that would have been exerted directly on the target in the absence of medium attenuation. Medium nonlinearity may also affect the radiation force [13]. Vibro-acoustography beamforming including medium attenuation and nonlinearity is an ongoing research.

A sector array transducer was modeled through linear acoustics in vibro-acoustography by the first time. The ultrasound beam produced by this transducer is described by Eqs. (21), (22) and (23). From these expressions we evaluated the vibro-acoustography PSF numerically for an 8-element sector array. Results showed that the PSF sidelobes are circularly distributed in eight spots around the mainlobe. The sidelobe levels are under -16 dB. Effects of sidelobes on vibro-acoustography images are still under investigation. The transverse resolution of the system is about 1.6×1.6 mm. Experimental results are in remarkable agreement with the theory.

In conclusion, sector array transducers can be suitable for vibro-acoustography applications producing localized sidelobs below -16 dB. Though the spatial resolution of current work is not remarkable, it can be improved by increasing the driving frequencies of the transducer.

Acknowledgments

The authors would like to thank Mr. Randall Kinnick for his help in the experimental arrangements. This work was partially supported by grants DCR013.2004-FAPEAL/CNPq (Brazil), CNPq 55.2076/02-3 (Brazil) and NIH EB00535-02 (USA).

References

[1] M. Fatemi and J. F. Greenleaf, "Ultrasound-stimulated vibro-acoustic spectrography," *Science*, vol. 280, pp. 82–85, 1998.

[2] R. T. Beyer, "Radiation pressure - the history of a mislabeled tensor," *Journal of the Acoustical Society of America*, vol. 63, no. 4, pp. 1025–1030, April 1978.

[3] G. R. Torr, "The acoustic radiation force," *American Journal of Physics*, vol. 52, no. 5, pp. 402–408, 1984.

[4] C. P. Lee and T. G. Wang, "Acoustic radiation pressure," *Journal of the Acoustical Society of America*, vol. 94, no. 2, pp. 1099–1109, August 1993.

[5] M. Fatemi, J. F. Greenleaf, and A. Manduca, "Imaging elastic properties of biological tissues by low-frequency harmonic vibration," *Proceedings in the Institute of Electric and Electronics Engineers*, vol. 91, pp. 1503–1519, October 2003.

[6] M. Fatemi and J. F. Greenleaf, "Vibro-acoustography: an imaging modality based on ultrasound-stimulated acoustic emission," *Proceedings of the National Academy of Sciences of the United States of America*, vol. 96, pp. 6603–6608, June 1999.

[7] S. Chen, M. Fatemi, R. Kinnick, and J. F. Greenleaf, "Comparison of stress field forming methods for vibro-acoustography," *IEEE Transaction on Ultrasonics, Ferroelectrics, and Frequency Control*, vol. 51, no. 3, March 2004.

[8] G. T. Silva, J. F. Greenleaf, and M. Fatemi, "Linear arrays for vibro-acoustography: a numerical simulation study," *Ultrasonic Imaging*, vol. 25, pp. 1–17, April 2004.

[9] E. Konofagou, J. Thierman, and K. Hynynen, "The use of ultrasound-stimulated acoustic emission in monitoring of modulus changes with temperature," *Ultrasonics*, vol. 41, no. 2003, pp. 337–345, July 2003.

[10] P. J. Westervelt, "Acoustic radiation pressure," *Journal of the Acoustical Society of America*, vol. 29, no. 1, pp. 26–29, January 1957.

[11] J. C. Lockwood and J. G. Willette, "High-speed method for computing the exact solution for the pressure variations in the nearfield of a baffled piston," *Journal of the Acoustical Society of America*, vol. 53, no. 3, pp. 735–741, 1973.

[12] W. L. Nyborg, "Acoustic streaming due to attenuated plane waves," *Journal of the Acoustical Society of America*, vol. 25, no. 1, pp. 68–75, 1952.

[13] O. V. Rudenko, A. P. Sarvazyan, and S. Y. Emelianov, "Acoustic radition force and streaming induced by focused nonlinear ultrasound in a dissipative medium," *Journal of the Acoustical Society of America*, vol. 99, no. 5, pp. 2791–2798, July 1996.

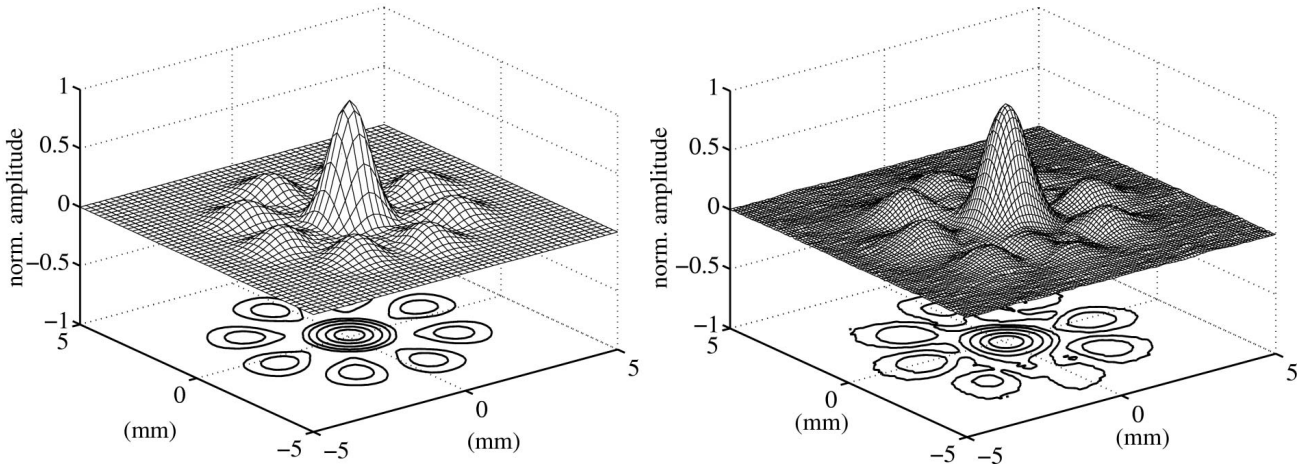

(a) Surface plot of the PSF with contour plot underneath.

(b) Surface plot of the measured PSF with contour plot underneath.

Figure 5. Theoretical and experimental PSFs.

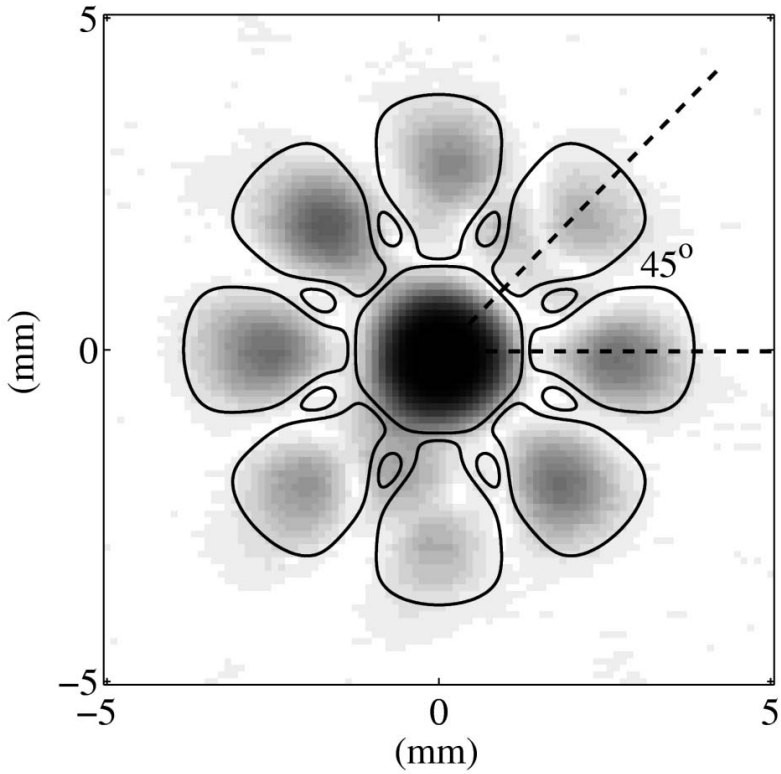

Figure 6. Image of the measured PSF. The contour lines are the theoretical PSF at -40 dB. The angle between the peak of two consecutive sidelobes is $\pi/4$ radians.